Tectonophysics 492 (2010) 201–212

Contents lists available at ScienceDirect

Tectonophysics

journal homepage: www.elsevier.com/locate/tecto

Crustal deformation associated with east Mediterranean strike–slip earthquakes: The 8 June 2008 Movri (NW Peloponnese), Greece, earthquake (M_w6.4)

Gerassimos A. Papadopoulos [a,*], Vassilis Karastathis [a], Charalambos Kontoes [b], Marinos Charalampakis [a], Anna Fokaefs [a], Ioannis Papoutsis [b]

[a] Institute of Geodynamics, National Observatory of Athens, Athens 11810, Greece
[b] Institute for Space Applications and Remote Sensing, National Observatory of Athens, Athens 15236, Greece

ARTICLE INFO

Article history:
Received 23 July 2009
Received in revised form 8 June 2010
Accepted 17 June 2010
Available online 27 June 2010

Keywords:
Strike–slip
Crustal deformation
Elastic dislocation
DInSAR analysis
Movri 2008 earthquake

ABSTRACT

The 2008 mainshock ($M_w = 6.4$) was the first modern, strong strike–slip earthquake in the Greek mainland. The fault strikes NE–SW, dips ~85°NW while the motion was right-lateral with small reverse component. Historical seismicity showed no evidence that the fault ruptured in the last 300 years. For rectangular planar fault we estimated fault dimensions from aftershock locations. Dimensions are consistent with that a buried fault was activated, lateral expansion occurred only along length and the rupture stopped at depth ~20 km implying that more rupture along length was favoured. We concluded that no major asperities remained unbroken and that the aftershock activity was dominated rather by creeping mechanism than by the presence of locked patches. For $M_o = 4.56 \times 10^{25}$ dyn cm we calculated average slip of 76 cm and stress drop $\Delta\sigma$~13 bars. This $\Delta\sigma$ is high for Greek strike–slip earthquakes, due rather to increased rigidity because of the relatively long recurrence (T>300 years) of strong earthquakes in the fault, than to high slip. Values of $\Delta\sigma$ and T indicated that the fault is neither a typical strong nor a typical weak fault. Dislocation modeling of a buried fault showed uplift of ~8.0 cm in Kato Achaia (Δ~20 km) at the hanging wall of the reverse fault component. DInSAR analysis detected co-seismic motion only in Kato Achaia where interferogram fringes pattern showed vertical displacement from 3.0 to 6.0 cm. From field-surveys we estimated maximum intensity of VIII in Kato Achaia. The most important liquefaction spots were also observed there. These observations are attributable neither to surface fault-breaks nor to site effects but possibly to high ground acceleration due to the co-seismic uplift. The causal association between displacement and earthquake damage in the hanging wall described for dip–slip faults in Taiwan, Greece and elsewhere, becomes possible also for strike–slip faults with dip–slip component, as the 2008 earthquake.

1. Introduction

A seismotectonic feature in the east Mediterranean region is the occurrence of large strike–slip earthquakes. Recent examples were the 1999 Izmit ($M_w = 7.4$) and Duzce ($M_w = 7.2$) earthquakes which ruptured in the western segment of the North Anatolian Fault with very clear surface fault-breaks (Reilinger et al., 2000; Duman et al., 2005). Historical sources provide documentation for the occurrence of large strike–slip earthquakes with surface fault-breaks along the Eastern Anatolian Fault and the Dead Sea Fault too (e.g. Guidoboni and Comastri, 2005; Daëron et al., 2007). Due to that those earthquakes have clear surface expressions, the crustal deformation patterns were studied not only by InSAR, GPS measurements and dislocation modeling but also by palaeoseismological and other geological methods.

Strike–slip faults associated with earthquakes of M~7.0 were observed in the Aegean Sea and the Ionian Sea as well (e.g. Drakopoulos and Ekonomides, 1972; Papazachos et al., 1984; Kiratzi et al., 1991; Taymaz et al., 1991; Louvari et al., 1999; Papadopoulos et al., 2001, 2003; Roumelioti et al., 2004). However, clues for the deformation patterns were provided only by the earthquake focal mechanisms due to that these earthquakes occurred under the sea and no submarine surveys were conducted so far. The only exception was the earthquake of 19 February 1968 ($M_s = 7.1$) which had surface fault expression in the Agios Efstratios Is., North Aegean Sea (Pavlides and Tranos, 1991).

On 8 June 2008, the strong mainshock that ruptured NW Peloponnese, along the Morvi Mountain foothills (Fig. 1) was the first modern, strong strike–slip earthquake occurring in the Greek mainland. Calculated seismic moment ranges from 3.10×10^{25} dyn cm to 6.50×10^{25} dyn cm (Table 1). Considerabe damage and ground failures were the two main elements of the macroseismic field. No strong, historical events were known to have occurred in the 2008 earthquake area. Therefore, there was a noteworthy lack of knowledge with respect to the crustal deformation of the area. In fact, neither focal mechanisms of significant earthquakes nor GPS measurements nor geologic offset were available until the occurrence of the 2008 earthquake. Consequently, that earthquake shed new light for the enhanced understanding of the

* Corresponding author.
E-mail address: papadop@gein.noa.gr (G.A. Papadopoulos).

0040-1951/$ – see front matter © 2010 Elsevier B.V. All rights reserved.
doi:10.1016/j.tecto.2010.06.012

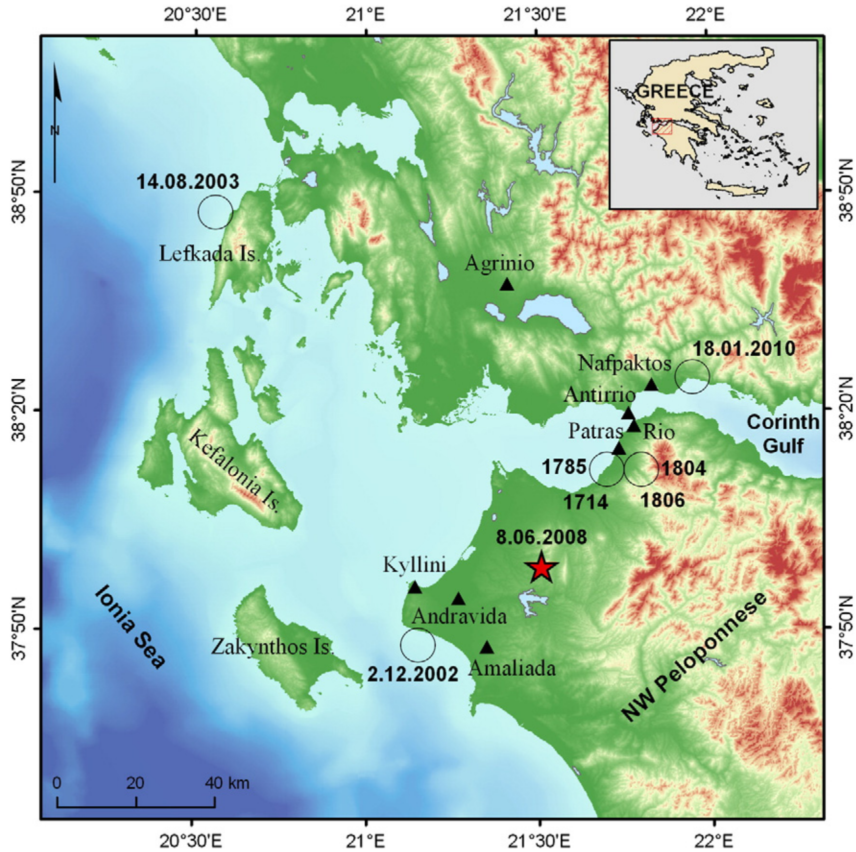

Fig. 1. Plots of epicenters (circles) of earthquakes discussed in the text. Historical earthquakes: 28 July 1714 (Ms6.3), 10 February 1785 (Ms6.4), 7 June 1804 (Ms6.4), 23 January 1806 (Ms6.2) (data after Papadopoulos et al., 2000). Recent earthquakes: 2 December 2002 (Mw5.6), 14 August 2003 (Ms6.2) and 18 January 2010 (Mw5.5) (epicenters after the earthquake catalogue of the National Observatory of Athens, http://www.gein.noa.gr/services/cat.html; magnitudes after the catalogue of Harvard (HRV), http://www.globalcmt.org/). Star illustrates the epicenter of the 2008 mainshock.

deformation associated with strike–slip earthquakes not only in the area of NW Peloponnese but in the entire Greek mainland.

In a geological study (Koukouvelas et al., 2009), the earthquake was attributed to a dextral, high-angle blind fault. Gallovič et al. (2009) found that predominantly unilateral rupture propagation to the north-east took place with two or three main patches. The major part of seismic moment, however, was released only in one patch. A study of the earthquake was also published by Ganas et al. (2009). A "storm" of four strong mainshocks (M_w>6) occurring in Greece in the

Table 1
Focal parameters and elements of the focal mechanism of the 8 June 2008 mainshock as determined by several seismological institutes. Key: φ_N^o = geographic latitude, λ_E^o = geographic longitude, h = focal depth, M_w = moment magnitude, M_o = seismic moment, HRV = Harvard University (USA), USGS = United States Geological Survey (USA), NOA = National Observatory of Athens (Greece), INGV = National Institute of Geophysics and Volcanology (Italy), ETHZ: Swiss Federal Institute of Technology Zurich, AUTH: Aristotle University of Thessaloniki (Greece).

$\varphi_N{}^\circ$	$\lambda_E{}^\circ$	h (km)	M_w	M_o (dyn cm)	Strike	Dip	Rake	Institute/ authors
37.93	21.63	24.7	6.4	4.56e+25	209	83	164	HRV (1)
38.15	21.59	10.0	6.3	3.10e+25	30	89	−160	USGS (2)
37.98	21.48	22.0	6.4	4.49e+25	210	82	175	NOA (3)
37.99	21.52	10.0	6.5	6.01e+25	210	85	179	INGV (4)
38.01	21.44	31.0	6.4	5.71e+25	213	81	165	ETHZ (5)
37.97	21.49	32.0	6.5	6.50e+25	29	89	−178	AUTH (6)

(1) http://www.globalcmt.org/.
(2) http://neic.usgs.gov/neis/eq_depot/2008/.
(3) http://bbnet.gein.noa.gr/MT.htm.
(4) http://www.bo.ingv.it/RCMT/searchRCMT.html.
(5) http://www.seismo.ethz.ch/mt/.
(6) http://geophysics.geo.auth.gr/the_seisnet/WEBSITE_2005/station_index_en.html.

first seven months of 2008 was examined and attributed to remote triggering effects (Papadopoulos et al., 2009). The Movri earthquake was one of the four mainshocks involved in the "storm".

To study the 2008 earthquake we were based on the space–time–size distribution of aftershocks, on modeling of the co-seismic elastic dislocation, on DInSAR analysis as well as on the evaluation of the earthquake effects. The possible causal link between the field of crustal deformation and the features of macroseismic field was also investigated and discussed. Previous studies of strong earthquakes in Greece and elsewhere based on similar approaches proved quite successful (e.g. Kontoes et al., 2000; Papadopoulos et al., 2004; Talebian et al., 2004; Kobayashi et al., 2009).

2. Historical seismicity and seismotectonic setting

Historical seismicity is of importance in studies of co-seismic ground deformation since it may provide information about ground failures associated with the earthquake activity. From an investigation in the rich historical earthquake record of western Greece it resulted that the earthquakes of 28 July 1714 (M_s = 6.3), 10 February 1785 (M_s = 6.4), 7 June 1804 (M_s = 6.4) and 23 January 1806 (M_s = 6.2) (Fig. 1) might be considered as regards its possible association with the fault zone activated with the 2008 earthquake. Based on documentary sources and on previous studies and catalogues (e.g. Mallet, 1853; Sathas, 1867; Galanopoulos, 1960, 1981; Papazachos and Papazachou, 1997; Spyropoulos, 1997; Ambraseys and Finkel, 1999), Papadopoulos et al. (2000) assigned maximum intensity of VIII, VIII–IX, IX and VII–VIII at Patras for the 1714, 1785, 1804 and 1806 earthquakes, respectively. A common feature of the four earthquakes is that apart from the damage caused in the today historical center of

Patras, damage was also noted away the 2008 fault zone. For example, in Nafpaktos town (Fig. 1) intensity as high as VIII was also experienced because of the 1714 shock. Therefore, Papadopoulos et al. (2000) located the four earthquakes in the area of Patras Gulf. Similar are the epicentral determinations by Papazachos and Papazachou (1997). Allowing for some error of no more than 20 km involved in the epicenters, we concluded that the evidence available disfavours the suggestion that the 1714, 1785, 1804 and 1806 earthquakes ruptured the fault segment activated with the 2008 earthquake.

The 2008 earthquake is the first to provide clear evidence about the stress-field dominating the area ruptured. Fault plane solutions (Fig. 2, Table 1) are consistent in that nearly pure dextral strike–slip motion occurred at depth. The preferred fault plane is a high-angle one dipping to NW with dip ranging from 81° to 89° and striking NE–SW, which is also the main direction of the aftershock zone. Small reverse component was involved in the seismic faulting.

From seismotectonic point of view the 2008 earthquake is a transition from the highly seismogenic areas of Patras Gulf and Corinth rift to the NE and the Ionian Sea to the SW (Fig. 1). Extensional stress-field striking nearly N–S prevails in the areas of Patras Gulf and Corinth rift (Doutsos et al., 1988). On the contrary, in the Ionian Sea to the SW extension of the 2008 rupture zone the stress-field becomes compressional along NE–SW (e.g. Louvari et al., 1999), which is due to the convergence between the African lithospheric plate and the southwestern termination of the Eurasian plate along the Hellenic Arc and Trench. However, several years ago a review on earthquake focal mechanisms and neotectonic observations showed that the fields of compression and extension are separated by a narrow zone of strike–slip motions which runs parallel to the Hellenic Arc (Papadopoulos, 1985). In fact, the rupture zones of both the 2008 and the $M_w = 5.6$ strike–slip mainshock of 2 December 2002 fall within that strike–slip zone (Fig. 1).

3. Aftershock activity and co-seismic deformation

The 2008 mainshock was followed by numerous aftershocks the locations of which were precisely determined by the seismograph network of the National Observatory of Athens (NOA; http://www.gein.noa.gr/services/cat.html) given that in the area affected by the earthquake the network is dense enough. Up to 16 November 2008 about 730 aftershocks were determined with local magnitude, M_L, ranging from 2.2 to 4.3. Statistically the magnitude, M_1, of the largest aftershock equals to $M - 1.2$ (± 1) (Båth, 1983), where M is the mainshock magnitude. This implies that the maximum magnitude observed in the 2008 aftershock sequence is rather low.

Dimensions of the seismic fault as well as of the aftershock area were determined from aftershock locations. The method which was introduced by Abe (1975) is simple and effective provided that accurate fault dimensions are calculated. The dimensions of the aftershock area and of the seismic fault were determined from lateral and vertical plots of aftershock locations determined by NOA and

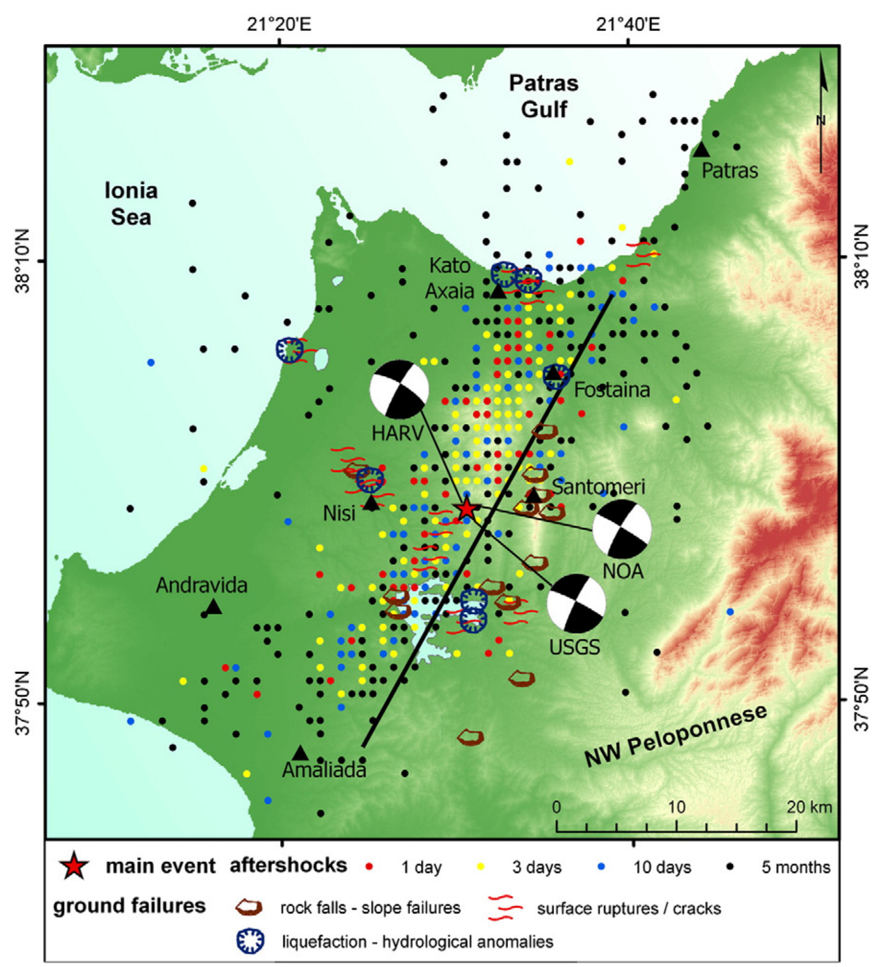

Fig. 2. The mainshock of 8 June 2008 (star) and its aftershocks (colour dots) recorded up to end of November 2008 (see text for details). Straight line is the hypothetical intersection of the fault surface with the Earth's surface. Beach-balls illustrate the earthquake focal mechanism determined by HRV, USGS and NOA (for explanations see Table 1). Localities and types of ground failures observed are shown.

occurring within 1-day, 3-day, 10-day and 5-month time intervals from the mainshock occurrence (Fig. 2). From the 1-day and 3-day plots the calculated aftershock zone length was found $L_c(1) \approx L_c(3) \approx 30$ km while the lateral aftershock zone width was $W_{cl}(1) \approx W_{cl}(3) \approx 10$ km. The final width W_{cl} did not changed in the 10-day and 5-month plots either, but the final length L_c increased to about 42 km. The aftershock area length, determined by aftershocks relocated by the double-difference method was found about 40 km (Gallovič et al., 2009) or 48 km (Ganas et al., 2009). The mainshock focal depth determined by NOA is 22 km. Gallovič et al. (2009) and Ganas et al. (2009) relocated the mainshock at depth 19 km and 18 km, respectively. Relocation results obtained from other authors are nearly identical with the locations produced by the NOA daily routine epicentral determinations, with the exception of the aftershock area length found by Ganas et al. (2009) which may be an overestimation.

Final dimensions of the aftershock area of about 42 km in length and 10 km in lateral width imply that some expansion occurred along length but not along width. The cloud of aftershock epicenters was clearly aligned along the NE–SW axis which is absolutely consistent with the strike of one of the two nodal planes indicated by the focal mechanism of the mainshock. Cross-section of the aftershock foci (Fig. 3) indicates that the uppermost ~5 km-thick layer, which very likely represents the sedimentary layers of the crust remained seismically inactive. This is consistent with the suggestion that the fault activated on 2008 was a blind one (Koukouvelas et al., 2009). The aftershock area did not exceed 25 km in depth. By considering that the focal depth of the mainshock was ~20 km and adopting a rectangular fault plane we assumed that the top and bottom depths of the seismic fault were 5 km and 20 km, respectively. Then, by considering a nearly vertical fault with an average dip of about 85° (Table 1), the down-dip width of the fault plane is $W_c = 15$ km.

Application of empirical relationships between mainshock magnitude and aftershock area for Mediterranean Sea earthquakes (Konstantinou et al., 2005) to the 2008 earthquake sequence, for a fault rupturing up to the surface, predict that $L_p = 33$ km, $W_{pl} = 13$ km and $W_p \approx 23$ km. Discrepancy between the calculated and the predicted dimensions of the fault plane is attributed to that the latter are based on the assumption that the fault ruptured up to the surface. This is not, however, in the former case, since there is geological evidence (Koukouvelas et al., 2009), strengthened by our aftershock observations, that a buried fault was activated. Then the rupture was extended from 5 km to 20 km, which very possibly is the brittle–ductile boundary, thus implying that more rupture along length of the fault was favoured. Verification comes from the seismic moment, M_o, formula:

$$M_o = \mu \cdot L \cdot W \cdot \bar{u} \tag{1}$$

where $\bar{u}$ (cm) = average slip in the source, and $\mu = 2 \cdot 10^{11}$ dyn/cm^2 is shear-modulus. All other things being equal, one may expect that the calculated and predicted aftershock areas, $A_c = L_c \cdot W_c$ and $A_p = L_p \cdot W_p$, should be equal. In fact, $A_c = 42\text{ km} \times 15\text{ km} = 630\text{ km}^2$ is not much different from $A_p = 33\text{ km} \times 23\text{ km} = 759\text{ km}^2$.

Properties of the aftershock sequence indicate that very likely no major asperities remained unbroken after the mainshock. In favour of this is that no remarkable lateral expansion of the aftershock area was observed, that only low magnitudes were involved in the aftershock sequence and that no large gaps were observed in the lateral distribution of the aftershock epicenters. We assumed, therefore, that nearly the total deformation was caused by the mainshock. To check further this suggestion we put forward the hypothesis that after the mainshock the fault zone was dominated by high degree of heterogeneity and asymmetrical stress distribution. In such geophysical conditions, which disfavour the presence of major asperities, one may expect high *b*-value to prevail as it was shown by pioneering laboratory experiments (Mogi, 1962; Scholtz, 1968). This was also verified from seismicity studies. For example, in Greece high *b*-value was calculated for the local seismicity associated with the very heterogeneous crustal structure of the volcanic region of Nisyros Is. (Papadopoulos et al., 1998). To verify further the hypothesis, we calculated the *b*-value in the Gutenberg and Richter (1944) relationship:

$$\log N(M \geq m) = a - bM \tag{2}$$

where N = cumulative number of earthquakes, M = magnitude, m = magnitude cut-off for data completeness, *a, b* are parameters. Theoretically $b = 1$ but this parameter is dependent on local seismotectonics, e.g. stress heterogeneity, presence or not of asperities. In fact, laboratory experiments, analysis of seismicity in mines and pore pressure records have shown that locally high stress can perturb the normal $b = 1$ to low values of 0.5 (Scholz, 1968; Wyss, 1973; Urbancic et al., 1992). On the contrary, creeping segments of the fault were found to be characterized by high *b*-values up to about $b \approx 1.5$ (Amelung and King, 1997). Therefore, for seismically active parts of the fault zone it was proposed that *b* can be used as an indicator where asperities may be located, that is where the creeping and locked patches are situated along the fault zone (Wyss et al., 2000, 2004, Wyss, 2001, Zhao and Wu, 2008).

Typical *b*-values for Greek background seismicity and aftershocks are around 1.0 (Papadopoulos et al., 1993) and 1.2 (Papazachos, 1971), respectively. We calculated *b*-value in the seismogenic area shown in Fig. 2 by applying the maximum likelihood approximation introduced by Aki (1965) and Utsu (1965):

$$b = \log e / [M] - m \tag{3}$$

where

$$[M] = \sum_{i=1}^{N} (M_i / N) \tag{4}$$

is the mean magnitude in the earthquake sample, and N is the number of events with magnitude $\geq m$. For reasons of data completeness the magnitude cut-off was taken as $m > 3.0$. A time period of 5 years before the 8 June 2008 mainshock was selected for the calculation of the *b*-value in the background seismicity. Selection of a longer time period results in an increase of m which is due to decreasing monitoring

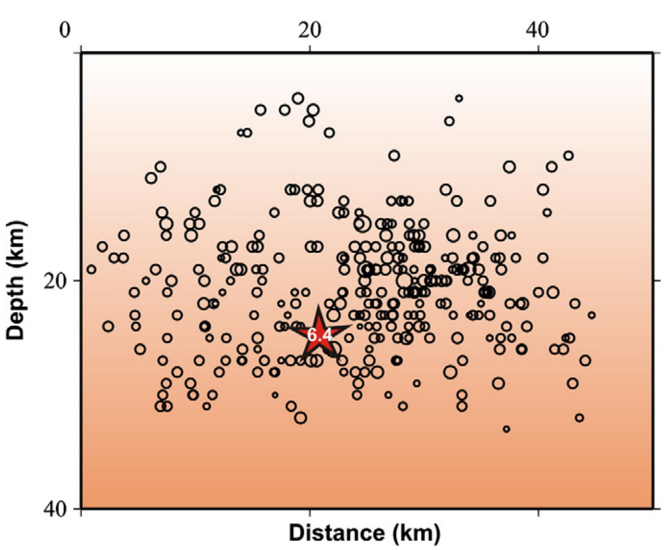

Fig. 3. Cross-section of the aftershock foci along fault strike (straight line in Fig. 2). Mainshock focus is also projected (star).

capabilities of the area as time goes back. Besides, the last strong earthquake in the area of NW Peloponnese before the occurrence of the 2008 mainshock was that of 2 December 2002 (M_w = 5.6) which was associated with foreshock and aftershock sequences. Therefore, the selection of a time period of no longer than 5 years before the 2008 mainshock secures the use of a catalogue segment which is not influenced by the 2002 sequence. The 5-year catalogue was declustered with a Greek version (Latoussakis and Stavrakakis, 1992) of the Gardner and Knopoff (1974) algorithm.

For background seismicity preceding by 5 years the 2008 mainshock we found b = 1.55. However, much higher b-values of 2.25, 1.89 and 1.77 were found for the 1-day, 10-day and 5-month aftershock periods, respectively. This result, verifies the assumption that no major asperities remained unbroken after the mainshock. These features make the 2008 aftershock sequence different from other Greek sequences associated with the same type of faulting and nearly the same mainshock magnitude. For example, the Lefkada mainshock (M_w = 6.2) of 14 August 2003 which ruptured in the Ionian Sea, was associated with dextral strike–slip faulting producing aftershocks of maximum M_w = 5.2 and of b = 1.1, with epicenters spatially distributed in two clusters separated by a 15-km-long asperity (Papadopoulos et al., 2003).

4. Modeling of co-seismic ground displacement

The field of static, co-seismic ground displacement caused by the 2008 earthquake was modelled by applying the dislocation model in an elastic half-space (Okada, 1985) by utilizing the Mirone (ver. 1.4.0) framework tool (Luis, 2007). We calculated ground displacement, d, as either uplift or subsidence. Strike, dip and slip for the preferred fault plane were adopted from the centroid-moment tensor solution of Harvard which determined magnitude M_w = 6.4 (Table 1). Focal depth of h = 20 km was adopted for the mainshock. Displacement amplitude, however, is sensitive to seismic moment and, hence, to variations of the average slip in the source. Average slip, $\bar{u}$, was calculated from Eq. (1) for three seismic moment estimates corresponding to M_w = 6.3, M_w = 6.4 and M_w = 6.5, respectively (Table 1). Length L_c (1) = 20 km and down-dip width W_c = 15 km were considered as fault dimensions. It was found that seismic slip $\bar{u}$ equals to 108 cm, 76 cm and 56 cm for $M_o = 6.50 \times 10^{25}$ dyn cm, $M_o = 4.56 \times 10^{25}$ and $M_o = 3.10 \times 10^{25}$, respectively. Then, absolute d values ranged from −9.4 to +11.4 cm for M_w = 6.5, and from −4.9 to +5.9 for M_w = 6.3, where (−) and (+) denote subsidence and uplift, respectively. For our preferred magnitude estimate of M_w = 6.4 the displacement d ranged from −6.6 to +8.0 cm, the maximum displacement amplitude being equal to 14.6 cm.

From the ground displacement field (Fig. 4) it comes out that uplift occupied the NW and SE parts of the rupture zone while subsidence was observed in the NE and SW parts. The maximum displacement amplitude was found in Kato Achaia in the NW part of the dislocation field, which is situated at the hanging wall domain of the reverse component of the fault motion.

Calculation of the static stress drop is of particular importance for understanding the mode of deformation and mechanical aspects of the 2008 seismic fault. Assuming a simple rectangular planar fault, the average static stress drop $\Delta\sigma$ was calculated from

$$\Delta\sigma = C\mu(\bar{u}/W_c) \tag{5}$$

The nondimensional constant C is taken as $C = 2/\pi$ for rectangular surface strike–slip fault (Knopoff, 1958) and as $C = 4/\pi$ for rectangular buried strike–slip fault (Aki, 1972) which is the present case. For average seismic slip $\bar{u}$ of 108 cm and of 56 cm, stress drop values of 18.4 and 8.8 bars were found, respectively. For our preferred seismic slip of 76 cm, $\Delta\sigma$ = 13 bars was calculated. In strong, strike–slip earthquakes occurring

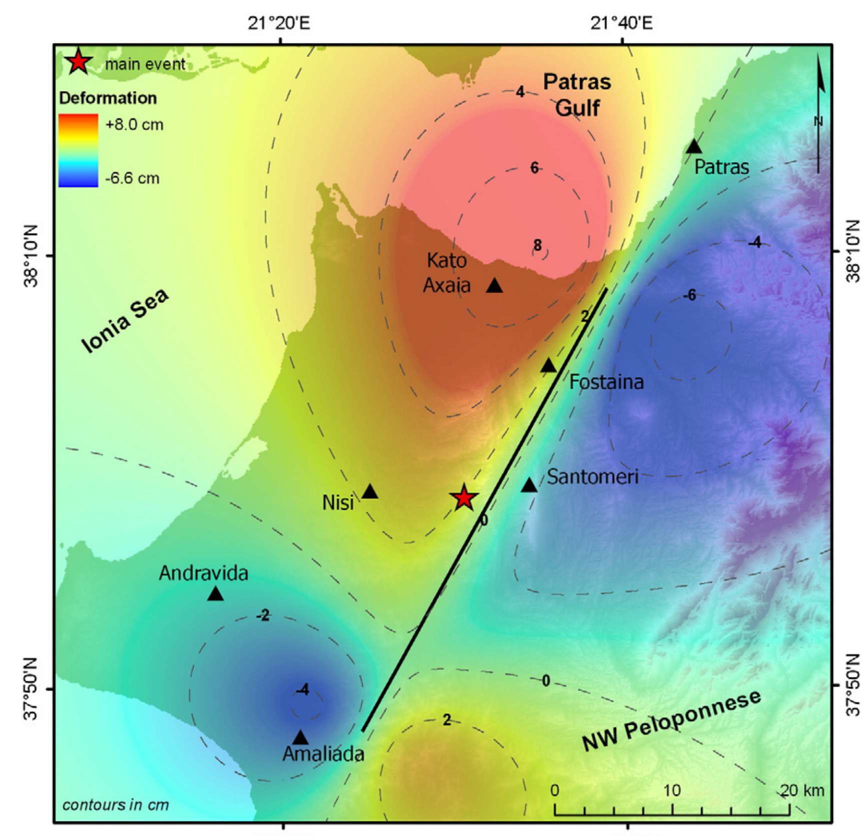

Fig. 4. The field of vertical co-seismic ground deformation caused by the 8 June 2008 mainshock. Dislocation modeling was performed for mainshock magnitude M_w = 6.4 (see text for details). Negative deformation means subsidence, otherwise uplift is meant. Maximum amplitude of deformation (uplift) by ~8.0 cm is observed in the area of Kato Achaia.

in the North Aegean Sea lower stress drop has been determined as a rule (e.g. Kiratzi et al., 1991). In the Ionian Sea, we applied Eq. (5) with $C=4/\pi$ and calculated stress drop for the strike–slip Lefkada Is. earthquake of 14 August 2003 for two alternative seismic fault dimensions suggested by Papadopoulos et al. (2003) and Benetatos et al. (2007). Nearly similar results were obtained for the two alternatives: $\bar{u}\sim 20$ cm and $\Delta\sigma\sim 3.5$ bars, which is lower than that found for the 2008 earthquake.

Large Pacific Ocean earthquakes are characterized, on the average, by $\Delta\sigma\approx 30$ bars and $L\approx 2$ W, independently on the earthquake size (Abe, 1975). For major earthquakes $\Delta\sigma\approx 60$ bars and $L\approx 2$ W. Kanamori and Anderson (1975) also found that $\Delta\sigma\approx 30$ bars, $\Delta\sigma\approx 100$ bars and $\Delta\sigma\approx 60$ bars for interplate, intraplate and "average" earthquakes, respectively. For intraplate earthquakes it was found that $\Delta\sigma$ ranges between 2 and 70 bars (Richardson and Solomon, 1977). Based on a much higher number of global observations, Allmann and Shearer (2009) found that $\Delta\sigma$ estimates for individual earthquakes range from about 3 to 500 bars, but the median stress drop of ~40 bars does not vary with moment, implying earthquake self-similarity over the $M_w=5.2$ to 8.3 range of their data. They found also a dependence of median stress drop on focal mechanism, with a factor of 3–5 times higher $\Delta\sigma$ for strike–slip earthquakes and with a factor of 2 times higher $\Delta\sigma$ for intraplate earthquakes compared to interplate ones. The Movri earthquake is discussed later as for its $\Delta\sigma$ in relation to fault mechanics.

5. DInSAR processing

DInSAR analysis is a well established technique (Massonet and Feigl, 1998) for remotely sensing co-seismic ground deformation. The method requires a pair of SAR scenes, depicting the affected area of interest, and the corresponding Digital Elevation Model (DEM) of the region. The processing of the phase of the complex input data results in a Line Of Sight (LOS) ground displacement pattern, represented in the final interferometric product as a set of deformation fringes.

Regarding the distressed area of NW Peloponnese, 21 ENVISAT SAR scenes were obtained from the European Space Agency (Table 2). These came from two adjacent parallel ENVISAT satellite tracks in both descending and ascending modes of operation (asc. tracks 186, 415 and desc. tracks 279, 50). The DEM used was created by combining Shuttle Radar Topography Mission (SRTM) elevation data with a higher quality DEM, which was derived from the digitization of the 20 m-contour lines from 1:50,000 topographic maps. Moreover, the interferometric processing of the SAR data was performed using the ROI-PAC (2008) and DIAPASON (CNES, 1996) software packages. Finally, the exact SAR sensor position for all the acquired scenes became available through the precise satellite orbit state vectors, provided by ESA DORIS system. Hence, using the above data and set of tools 51 interferograms were compiled (Papoutsis et al., 2008) in an attempt to map the ground displacement incurred by the 2008 mainshock. Fig. 5 shows the baselines of the interferograms.

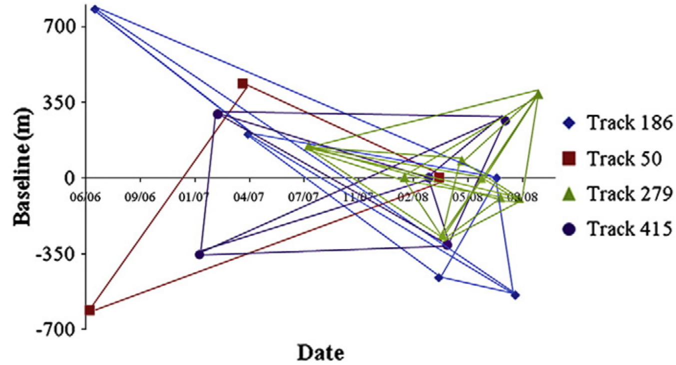

Fig. 5. Perpendicular baselines of the SAR pairs used for the generation of the interferograms.

The area of NW Peloponnese is quite challenging to perform a DInSAR analysis, as it is highly vegetated. This induced significant temporal signal decorrelation and thus the coherence between the scenes was degraded (Fig. 6a). To suppress decorrelation noise a procedure involving a two-stage process was adopted. Firstly, the two interferograms with the best coherence statistics were identified and stacked, in order to obtain their mean phase values for each pixel. This step presumed the accurate geo-referencing of the interferograms. Secondly, a 3×3 pixels rectangular averaging window was applied as a smoothing filter to constrain the noise to an acceptable level, with simultaneous spatial resolution degradation.

A typical co-seismic stacked interferogram (Fig. 6b) was formed by using the interferometric pairs created from three ENVISAT SAR scenes with orbit numbers 30894 and 32397 in the pre-seismic stage and 32898 in the post-seismic stage. For the 30994–32898 co-seismic pair the perpendicular baseline was 3 m, whereas for the 32397–32898 pair the corresponding value was 80 m. In this stacked interferometric product it is obvious that there is no typical co-seismic deformation fringe pattern, as one would expect for an earthquake of relatively high magnitude. This is in accordance with that the earthquake focus was relatively deep and the activated fault was a blind one. However, in a closer look to the Kato Achaia area, a set of fringes with limited extent emerged (Fig. 6c). This fringe pattern was not observed in any of the available pre-seismic (Fig. 6d, formed by scenes 31896–32397 with perpendicular baseline of 345 m) or post-seismic interferograms. In addition, these fringes could not be associated with DEM errors not only due to that the area is relatively flat, the average Altitude of Ambiguity being sufficiently high (~65 m), but also because the fringes are absent in both the pre-seismic and post-seismic interferograms with even lower Altitude of Ambiguity. Moreover, they cannot be attributed to atmospheric and/or tropospheric disturbances which usually show strong spatial correlation and hence they appear as uniformly colored areas. If they were attributed to atmospheric disturbances of the signal in any of the images used, they would also appear in all pre-seismic and post-seismic interferograms created using the same image. Nonetheless, this was never observed. Lastly, the detected fringes can neither be linked with orbital errors, as these would create vertical fringes of linear type crossing the interferogram from north to south.

Table 2
ENVISAT scenes acquired in NW Peloponnese (ASAR Image Mode, Swath 2, Incidence angle 29°, VV Polarisation).

No.	Orbit	Date	Flight direction	Track
1	22785	09/07/2006	Ascending	186
2	26793	15/04/2007	Ascending	186
3	31803	30/03/2008	Ascending	186
4	33306	13/07/2008	Ascending	186
5	33807	17/08/2008	Ascending	186
6	22649	30/06/2006	Descending	50
7	26657	06/04/2007	Descending	50
8	31667	31/03/2008	Descending	50
9	28389	05/08/2007	Descending	279
10	30894	27/01/2008	Descending	279
11	31896	06/04/2008	Descending	279
12	32397	11/05/2008	Descending	279
13	32898	15/06/2008	Descending	279
14	33399	20/07/2008	Descending	279
15	33900	24/08/2008	Descending	279
16	34401	28/09/2008	Descending	279
17	25519	16/01/2007	Ascending	415
18	26020	20/02/2007	Ascending	415
19	31531	11/03/2008	Ascending	415
20	32032	15/04/2008	Ascending	415
21	33535	29/07/2008	Ascending	415

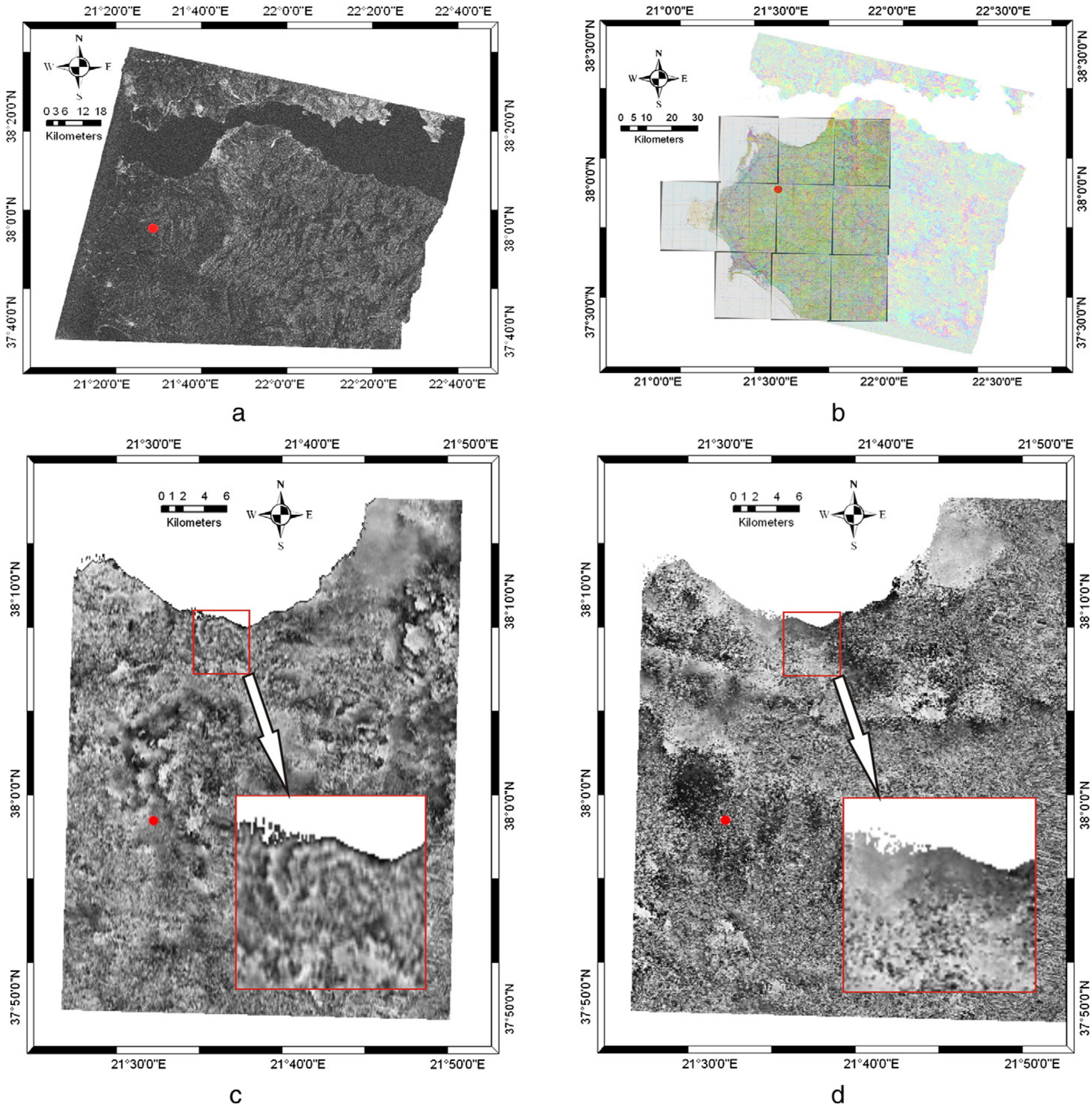

Fig. 6. (a) Coherence map of the affected area. White stands for high coherency while black for low. (b) Co-seismic stacked interferogram project on a political map. Altitude of ambiguity is 65 m. (c) Zoom of the previous co-seismic stacked interferogram in the Kato Achaia area, to highlight the fringe pattern. (d) Pre-seismic interferogram with 29 m altitude of ambiguity. The dot is the mainshock epicenter, while the box confines the Kato Achaia area.

The low coherency values that are dominant in Kato Achaia prevent us from making accurate estimation of the deformed area. However, one can confidently suggest that an area of about 35 to 40 km^2 presented a LOS ground movement of about one to two fringes (Fig. 6c). This is equivalent to LOS uplift from 2.8 cm to 5.6 cm or, assuming that the displacement is purely vertical, from 3.0 cm to 6.0 cm vertical uplift, taking into consideration the 23° incidence angle, which is absolutely consistent with the amplitude of vertical displacement calculated by the elastic dislocation modeling.

6. The macroseismic field

Studies performed in several seismogenic areas of the world have shown that seismic ground motion and the patterns of earthquake damage can be correlated with the faulting parameters and the co-seismic displacement. There is observational evidence that the seismic motion of the hanging wall of the seismic fault is larger than that of the footwall for dip–slip earthquakes (e.g. Allen et al., 1998). Numerical simulation results indicated that the particle motions on the hanging wall are larger than those on the footwall, and that particle motions decrease rapidly on the footwall and less rapidly on the hanging wall (Shi et al., 2003). In the vicinity of the seismic fault outcrop, the particle motion increases rapidly, both on the hanging wall and footwall. Chang et al. (2004) showed that accelerometric records of the 1999 Chi-Chi, Taiwan, earthquake ($M_w = 7.6$), from sites on the hanging wall exhibit larger acceleration than those from the footwall, that these effects cannot be simply accounted for by a proper choice of distance metric and that rather, seismic waves trapped in the hanging wall wedge may have been involved. For the same earthquake it was found that the surface damage was predominantly caused by co-seismic deformation (Shieh et al., 2001).

In Greece, the static displacement field of the Athens 1999 earthquake ($M_w = 5.9$) associated with normal faulting was determined by numerical dislocation modeling and by analysis from InSAR images (Papadopoulos et al., 2004). Consistent results were obtained from the two approaches: maximum amplitude of vertical displacement was found in the hanging wall equal to 7 cm for a fault that reaches the surface and to 1.8 cm for a blind fault. It was found also that the macroseismic field pattern is controlled by the static displacement pattern. The majority of the highest seismic intensities were distributed within the hanging wall but very close to the fault, with a gradual decrease with the distance from the fault. Because of this, the hypothesis was made that in dip–slip earthquakes the characteristics of the static displacement predicts well enough the characteristics of the macroseismic field, although ground displacement is dominated by relatively low frequency as compared to the ground acceleration. This hypothesis was verified later by Fokaefs (2007) who examined systematically more Greek earthquakes of normal faulting.

There is no clear evidence that the correlation described above for dip–slip earthquakes is also valid for strike–slip earthquakes. The involvement of a small reverse component in the faulting of the 2008 mainshock motivated the examination of such a possible correlation. We analysed the main elements of the 2008 macroseismic field, that is ground failures and building damage. In the next section we discuss them with regard to its possible correlation with the ground deformation pattern. Particular attention was given in Kato Achaia since both elastic dislocation modeling and DInSAR analysis showed some uplift anomaly there.

In two post-event field-surveys performed during the first week following the mainshock we observed (Fig. 2) surface fault-breaks, ground fissures and cracks, rockfalls and liquefaction in soil in many observation points (Papadopoulos et al., 2008). Similar observations were published by others as well (e.g. Kokkalas et al., 2008; Lekkas et al., 2008; Papathanassiou et al., 2008; Koukouvelas et al., 2009; Ganas et al., 2009).

Three are the main surface fault-breaks observed: the Nisi, Michoi and Vithoulkas ones, having lengths of 5–6 km and vertical offset on the order of 25 cm, 10 cm and 5 cm, respectively (Koukouvelas et al., 2009). It remains doubtful, however, if they (e.g. in Fig. 7a) represent surface expressions of the seismic fault segment activated in depth. In fact, none of the fault-breaks follow the NE–SW strike of the seismic fault. Besides, the surface fault-breaks were tectonically attributed to an upwards partitioning of a buried strike–slip fault into several minor faults (Koukouvelas et al., 2009). Observations in Italy have shown that even in cases where surface ruptures concentrate in narrow bands along the fault direction, they are not always the direct result of primary rupture at depth (e.g. Cinti et al., 1999). In Bam, Iran, the main rupture of the 2003 earthquake did not occur on faults beneath the obvious surface traces, but on a fault further west, in a region where there is a complete absence of surface features (Talebian et al., 2004). Similarly, very fresh results from palaeoseismological trenching showed that (Zygouri et al., submitted for publication) the Nisi surface fault-break should not be attributed to a gravity-driven rupture, as suggested by Ganas et al. (2009), but it should be genetically related to an unknown seismotectonic structure with an average late Quaternary slip rate of 1.5 mm/yr.

In the train station of Kato Achaia clear bending of the WNW–ESE trending railway was observed (Fig. 7b), which should not be attributed to co-seismic surface break given that no ground break, fissure or crack were observed on either sides of the railway. Our favoured explanation is that the railway bending was due to the vibration caused by surface waves of *SH* type. This is a physically plausible explanation since during the passage of the horizontally polarized *S* waves (*SH*) all particles of the substance move horizontally. Then, the railway bending does not provide information about the geometry and kinematics of the seismic fault at depth. Ground fissures and cracks observed in other observation points (Fig. 2) are of no tectonic importance since they were caused by local openings of loosed surface material.

Fig. 7. Ground breaks near the west bank of Vergas River (a; photo courtesy by G.A. Papadopoulos). Railway bending observed in the Kato Achaia train station after the earthquake (b; photo courtesy by I. Koukouvelas). Our favoured explanation is that railway bending is due rather to horizontal ground shaking because of SH waves than to surface fault-break.

Liquefaction in soil were observed in several points mainly along the earthquake rupture zone (Fig. 2). The most extensive liquefaction was produced in two spots of the Kato Achaia coastal area at epicentral distance of $\Delta\sim 20$ km. Surface manifestations of liquefaction included sand boils and ejections of water mixed with soft sand along numerous ground fissures and local depressions (Fig. 8a). Massive rockfalls occurred particularly along the Movri mountainous village of Santomeri (Fig. 8b). Isolated rockfalls occurred also in other localities.

The maximum epicentral distance, R_e, at which liquefaction or rockfall may occur, is a function of the earthquake magnitude M_s or M_w. Maximum distance, R_e, at which liquefaction and rockfalls were observed are ~27 km and 18 km (Fig. 1), respectively, which fall clearly within the respective limiting distances of 52 km and 66 km predicted by empirical M_s/R relationships for $M_s\approx M_w=6.4$, which is the mainshock magnitude:

$$1.584\log R_e = -3.686 + M_s,\ M_s\geq 5.9 (R_e\ \text{in km}) \tag{6}$$

for liquefaction in soil (Papadopoulos and Lefkopoulos, 1993) and

$$\log R_e = -2.98 + 0.75M_s,\ M_s\geq 5.3\ (R_e\ \text{in km}) \tag{7}$$

for landslides and rockfalls (Papadopoulos and Plessa, 2000).

Damage was observed particularly in single-house buildings in many villages of the Elia and Achaia provinces but no massive building collapses were reported. Two persons were killed and about 265 were injured. Total or partial collapse was observed in tenths of single, mainly old non-reinforced concrete, one-storey houses and other buildings, such as churches, particularly in the villages of Nisi, Valmi, Fostaina, and Santomeri. In these villages we assigned macroseismic intensity VII or VII+ at maximum in the EMS-98 scale. Damage was also caused in residential and other buildings in important cities, such as Patras and Amaliada, situated to the north and south ends of the rupture zone, respectively. Noticeable damage was also caused in the industrial zone of Patras, e.g. in a brewery factory at $\Delta\sim 20$ km, where the predominant destruction was the collapse of three silot bearing weight of 1500 t each (Fig. 9a). However, the highest intensity of VIII degree was assigned to Kato Achaia given that many masonry buildings and several concrete-

Fig. 9. Collapse of three silots in a brewery factory in the industrial zone of Patras (a) and partial collapse of house building in the Kato Achaia town (b) (photo courtesy by G.A. Papadopoulos).

Fig. 8. Ground break and sand blows due to liquefaction in soil near the coastal zone of Kato Achaia (a; photo courtesy by I. Koukouvelas). Rockfall near Santomeri village (b; photo courtesy by G.A. Papadopoulos). The size of the rock is 2.7 m in height and 2.9 m in width.

reinforced buildings suffered serious damage or even damage beyond repair (Fig. 9b).

7. Discussion

The determination of the seismic fault dimensions and of the co-seismic slip is of critical importance since other parameters and calculations depend directly on them. We selected best estimates for the fault dimensions based on both the routine aftershock determinations of NOA and the relocations performed by others. The co-seismic uplift detected in Kato Achaia by elastic dislocation modeling was verified from DInSAR analysis, which is a strong evidence that the fault dimensions and other parameters introduced in the dislocation modeling are correct. The fringe pattern in the interferogram from which the co-seismic uplift in Kato Achaia becomes evident, is true for a number of reasons explained in Section 5. For a preferred seismic moment $M_o = 4.56 \times 10^{25}$ dyn cm ($M_w = 6.4$) stress drop of $\Delta\sigma = 13$ bars was found which is relatively high for Greek strike–slip earthquakes. This may be due rather to relatively increased rigidity, as a possible result of the long repeat time of earthquakes in the area of the 2008 earthquake, than to high seismic slip in the fault. It is appropriate to discus here the classification of the seismic fault of 2008 earthquake in relation to the repeat time of strong earthquakes on it. Kanamori and Allen (1986) have related differences in $\Delta\sigma$ for large earthquakes to their repeat times, T. For $M_w = 6.4$, fault length $L = 20$ km, fault width $W = 11$ km and intermediate $\Delta\sigma$, which are exactly the parameters of the 2008 earthquake, the expected T ranges from 300 to 2000 years. Very likely no strong earthquake ruptured the 2008 Movri fault at least in the last 300 years. Romanowicz and Ruff (2002) examined the moment-length scaling of large strike–slip earthquakes in relation to the strength of faults and found that most continental interplate strike–slip earthquakes occur on weak faults, and most events on relatively old oceanic crust or in intraplate settings occur on strong faults. They concluded that earthquakes with T occur on stronger faults, and result in larger moments than earthquakes with shorter T, for the same length of rupture.

A possible explanation for the $\Delta\sigma$ differences between intraplate and interplate earthquakes come from numerical simulations of faults (Kato, 2009). Namely, in a model intraplate fault assumed to be loaded uniformly, $\Delta\sigma$ is uniform over the fault with a larger average value. On the contrary, stress concentration is generated at a plate boundary region between locked area and aseismic sliding area for a model interplate earthquake. This stress concentration hastens earthquake occurrence, resulting in lower average $\Delta\sigma$ (Kato, 2009). Allmann and Shearer (2009) speculated that the cause for the observed stress drop variations of $\Delta\sigma$ may be due to possible mechanisms such as lateral variations in rigidity, variations in the material between different plate boundaries, and variations in the absolute values of the principal stresses or the orientation of plate boundaries with respect to the direction of the principal stresses.

In the above context, the fault of Movri earthquake was neither a typical weak nor a typical strong fault. In the classification of Kanamori and Allen (1986) the T's in weak faults are less than 300 years while in strong faults T's exceed 2000 years. In this scheme the Movri seismic fault could be considered as a strong one. However, assuming that the Movri earthquake was of the continental interplate type, one may expect a rather weak fault according to Romanowicz and Ruff (2002). But the interpretation they proposed in terms of differences in $\Delta\sigma$ is clear only for events with $M_o > 0.50 \times 10^{27}$ dyn.cm. For smaller events, such as the Movri earthquake, even though the average $\Delta\sigma$ is higher in intraplate than in interplate settings, the dispersion in the data is very large. This may be due to the proportionately larger variability in fault width and strength for smaller events.

Elastic dislocation modeling and DInSAR analysis have shown that in Kato Achaia, situated at $\Delta \sim 20$ km in the field of uplift at the hanging wall domain of the reverse fault component, constitutes a spot of maximum vertical co-seismic displacement. At the same time, Kato Achaia is a spot of maximum seismic intensity. This coincidence could not be explained neither by surface fault-breaks nor by site effects.

In the light of the findings in Greece, Taiwan and elsewhere that in dip–slip faults seismic ground motion and the patterns of earthquake damage can be correlated with the faulting parameters and the co-seismic displacement, one may argue that the co-seismic uplift detected in Kato Achaia was the main factor that contributed for the maximum intensity to be felt there. Unfortunately, no accelerometric data are available from Kato Achaia. Peak ground acceleration PGA = 0.237 g was recorded in Amaliada ($\Delta \sim 20$ km) to the SW (NOA, http://www.gein.noa.gr/English/new-accelnet-eng/list-of-earthquakes.htm). The nearest to Kato Achaia PGA's were recorded in Patras ($\Delta \sim 35$ km) to the NE: 0.16 g (NOA, http://www.gein.noa.gr/English/new-accelnet-eng/list-of-earthquakes.htm) 0.13, 0.11 and 0.09 g (ITSAK, http://www.itsak.gr/documents/AchaiaIlia/Achaia-Ilia_Jun2008_2ndReport.pdf). Application of an empirical rule (Ambraseys, 1988), which predicts the critical ground acceleration, K_c, needed to cause liquefaction as a function of magnitude and distance inserted in Eq. (6), showed that for the liquefied site of Kato Achaia beach $K_c \approx 0.08$ g, which is the minimum PGA that one may expect in Kato Achaia.

8. Conclusions

The mainshock of 8 June 2008 was the first modern, strong strike–slip earthquake in the Greek mainland. Therefore, it is of particular importance for understanding better the co-seismic deformation associated with strike–slip earthquakes in the east Mediterranean Sea. The causative fault was striking NE–SW and dipping ~85°NW. It was of right-lateral slip with small reverse component. This fault acts as a transition between the extensional area of Patras Gulf–Corinth rift and the compressional area of the Ionian Sea. There is no historical evidence that the 2008 fault segment was ruptured by strong earthquake in at least the last 300 years.

The uppermost crustal layer of ~5 km remained seismically inactive, while the aftershock focal depths did not exceed 25 km. These observations are consistent with geological field observations (Koukouvelas et al., 2009) indicating that a buried fault was activated with the mainshock.

Assuming a rectangular planar seismic fault, we estimated fault dimensions: mainshock rupture $L = 20$ km; aftershock area length $L_c \approx 42$ km; lateral aftershock zone width $W_{cl} \approx 10$ km; mainshock focal depth, $h = 20$ km; seismic fault depth ranging from 5 km to 20 km; down-dip width $W = 15$ km. The above figures indicate that some lateral expansion occurred only along length. The aftershock area length is notably larger than the one (~33 km) expected from empirical relationships. Since the seismogenic layer was ruptured from the depth of 5 km to about 20 km, very possibly up to the brittle–ductile transition, more rupture along length was favoured.

The low aftershock magnitudes ($M_L \leq 4.3$), that no remarkable lateral gap in the earthquake epicenters was noted and that no significant lateral expansion of the aftershock area occurred, could be interpreted with that no major asperities remained unbroken after the mainshock. This is consistent with the unusually high b-value (= 2.25) found particularly in the early stage of the aftershock activity, which indicates rather creeping mechanism than the presence of locked patches. We assume, therefore, that nearly the total deformation of the sequence was caused by the mainshock.

Average co-seismic slip of 76 cm and static $\Delta\sigma = 13$ bars were found for a preferred mainshock seismic moment of $M_o = 4.56 \times 10^{25}$ dyn cm ($M_w = 6.4$). This $\Delta\sigma$ value is less by 2–3 times than the world median value but higher than the $\Delta\sigma$ in strong strike–slip earthquakes in the North Aegean Sea and the Ionian Sea. The higher $\Delta\sigma$ is attributed rather to increased fault rigidity than to increased seismic slip. Increased fault rigidity is consistent with the relatively long repeat time of strong earthquakes in the Movri fault which very possibly exceeds 300 years. From this point of view that fault is a strong one. Assuming, however, that the 2008 earthquake was of the continental interplate type, one may expect a rather weak fault. We conclude that the fault was neither a typical weak nor a typical strong fault.

Dislocation modeling of a buried fault in an elastic half-space showed maximum uplift of about 8.0 cm in the Kato Achaia area ($\Delta \sim 20$ km) at the hanging wall of the reverse component of fault motion in the NW part of the aftershock area. No co-seismic movement was detected by DInSAR analysis with the exception of the Kato Achaia area where again vertical ground displacement ranging from 3.0 cm to 6.0 cm was calculated.

The most important spots of liquefaction caused by the earthquake were observed in the Kato Achaia Beach. We estimated maximum seismic intensity of VIII degree (EMS-98 scale) in Kato Achaia which is attributable neither to surface fault-breaks nor to site effects. An explanation is the possibly high ground acceleration of >0.08 g estimated in Kato Achaia due to the co-seismic uplift detected there.

From the spatial correlation found between the fields of intensity and of ground displacement for dip–slip earthquakes in Taiwan, Greece and elsewhere, it was suggested that the former is controlled by the latter. Although ground displacement is dominated by relatively low frequency as compared to seismic ground acceleration, the causal association between ground displacement and increased earthquake damage in the hanging wall of motion becomes possible not only for pure dip–slip earthquakes but also for strike–slip earthquakes with small dip–slip component, as the Kato Achaia case indicates for the 2008 earthquake.

Acknowledgements

This work was supported by the project SEAHELLARC, EU-FP6, contract 037004. ENVISAT SAR scenes were obtained from the ESA in the framework of the ESA-GREECE AO project 1489OD/11-2003/72. The first author is thankful to Dr J. Koukouvelas for his help and guidance in the field.

References

Abe, K., 1975. Reliable estimation of the seismic moment of large earthquakes. J. Phys. Earth 23, 381–390.
Aki, K., 1965. Maximum likelihood estimate of *b* in the formula log $N = a - bM$ and its confidence limits. Bull. Earthquake Res. Inst. Tokyo Univ. 43, 237–239.
Aki, K., 1972. Earthquake mechanism. Tectonophysics 13, 423–446.
Allen, C.R., Brune, J.R., Cluff, L.S., Barrows, A.G., 1998. Evidence for unusually strong near-field ground motion on the hanging wall of the San Fernando fault during the 1971 earthquake. Seismol. Res. Lett. 69, 524–531.
Allmann, B.P., Shearer, P.M., 2009. Global variations of stress drop for moderate to large earthquakes. J. Geophys. Res. 114, B01310. doi:10.1029/2008JB005821.
Ambraseys, N.N., 1988. Engineering seismology. Earthquake Eng. Struct. Dyn. 17, 1–105.
Ambraseys, N.N., Finkel, C., 1999. Unpublished Ottoman archival information on the seismicity of the Balkans during the period 1500–1800. Natural Disasters in the Ottoman Empire, Institute for Mediterranean Studies, Halcyon Days in Crete III, A Symposium held in Rethymnon, 10–12 January 1997. Crete University Press, pp. 89–107.
Amelung, F., King, G., 1997. Earthquake scaling laws for creeping and non-creeping faults. Geophys. Res. Lett. 24, 507–510.
Båth, M., 1983. The seismology of Greece. Tectonophysics 98, 165–208.
Benetatos, Ch., Dreger, D., Kiratzi, A., 2007. Complex and segmented rupture associated with the 14 August 2003 Mw 6.2 Lefkada, Ionian Islands earthquake. Bull. Seismol. Soc. Am. 97, 35–51.
Chang, T.-Y., Cotton, F., Tsai, Y.-B., Angelier, J., 2004. Quantification of hanging-wall effects on ground motion: some insights from the 1999 Chi-Chi earthquake. Bull. Seismol. Soc. Am. 94, 2186–2197.
Cinti, F.R., Cucci, L., Marra, F., Montone, P., 1999. The 1997 Umbria–Marche (Italy) earthquake sequence: relationship between ground deformation and seismogenic structure. Geophys. Res. Lett. 26, 895–898.
CNES, 1996. Philosophie et mode d'emploi de la chaine logicielle interferometrique DIAPASON. Toulouse, France.
Daëron, M., Klinger, Y., Tapponier, P., Elias, A., Jacques, E., Sursock, A., 2007. 12,000-Year-long record of 10 to 13 paleoearthquakes on the Yammoûneh Fault, Levant Fault System, Lebanon. Bull. Seismol. Soc. Am. 97, 749–771.
Doutsos, T., Kontopoulos, N., Poulimenos, G., 1988. The Corinth–Patras rift as the initial stage of continental fragmentation behind an active island arc (Greece). Basin Res. 1, 177–190.
Drakopoulos, J.C., Ekonomides, A.C., 1972. Aftershocks of February 19, 1968 earthquake in Northern Aegean Sea and related problems. Pageoph 95, 100–115.
Duman, T.Y., Emre, O., Dogan, A., Ozalp, S., 2005. Step-over and bend structures along the 1999 Duzce earthquake surface rupture, North Anatolian fault, Turkey. Bull. Seismol. Soc. Am. 95, 1250–1262.
Fokaefs, A., 2007. Surface deformation patterns associated with strong earthquakes of Greece. MSc Thesis, National and Kapodistrian University of Athens, Greece, 82 pp..
Galanopoulos, A.G., 1960. A catalogue of shocks with Io ≥ VI or M ≥ 5 for the years 1801–1958. Seismol. Lab. Univ, Athens.
Galanopoulos, A.G., 1981. The earthquake potential of Greece. Ann. Géol. Pays Hellén. 30, 648–724 (in Greek).
Gallovič, F., Zahradník, J., Křížová, D., Plicka, V., Sokos, E., Serpetsidaki, A., Tselentis, G.A., 2009. From earthquake centroid to spatial–temporal rupture evolution: Mw 6.3 Movri Mountain earthquake, June 8, 2008, Greece. Geophys. Res. Lett. 36. doi:10.1029/2009GL040283.
Ganas, A., Serpelloni, E., Drakatos, G., Kolligri, M., Adamis, I., Tsimi, Ch., Batsi, E., 2009. The Mw 6.4 SW-Achaia (Western Greece) earthquake of 8 June 2008: seismological, field, GPS observations, and stress modeling. Journal of Earthquake Engineering 13, 1101–1124.
Gardner, J.K., Knopoff, L., 1974. Is the sequence of earthquakes in Southern California, with aftershocks removed, Poissonian? Bull. Seismol. Soc. Am. 64, 1363–1367.
Guidoboni, E., Comastri, A., 2005. Catalogue of earthquakes and tsunamis in the Mediterranean area, 11th–15th century. Istituto Nazionale di Geofisica e Vulcanologia, Rome, p. 1037.
Gutenberg, B., Richter, C., 1944. Frequency of earthquakes in California. Bull. Seismol. Soc. Am. 34, 185–188.
Kanamori, H., Allen, C. R., 1986. Earthquake repeat time and average stress drop. In: S. Das, J. Boatwright & C. H. Scholz (Eds.) Earthquake Source Mechanics, Geophys. Monogr. 37, Maurice Ewing v. 6, Am. Geophys. Union, Washington, D. C., 227–235.
Kanamori, H., Anderson, D.L., 1975. Theoretical basis of some empirical relations in seismology. Bull. Seismol. Soc. Am. 65, 1073–1095.
Kato, N., 2009. A possible explanation for difference in stress drop between intraplate and interplate earthquakes. Geophys. Res. Lett. 36. doi:10.1029/2009GL040985.
Kiratzi, A.A., Wagner, G.S., Langston, C.A., 1991. Source parameters of some large earthquakes in Northern Aegean determined by body waveform inversion. PAGEOPH 135, 515–527.
Knopoff, L., 1958. Energy release in earthquakes. Geophys. J. 1, 44–52.
Kobayashi, T., Takada, Y., Furuya, M., Murakami, M., 2009. Locations and types of ruptures involved in the 2008 Sichuan earthquake inferred from SAR image matching. Geophys. Res. Lett. 36, 1–5.
Kokkalas, S., Xypolias, P., Koukouvelas, I.K., 2008. Surface ruptures of the Mw 6.3 (June 08, 2008) earthquake event in the Northwest Peloponnese. 31st General Assembly, European Seismological Commission, Hersonissos, Crete, Greece, 7–12 September 2008, Programme and Abstracts, p. 319 (abstr.).
Konstantinou, K., Papadopoulos, G.A., Fokaefs, A., Orfanogiannaki, K., 2005. Empirical relationships between aftershock area dimensions and magnitude for earthquakes in the Mediterranean Sea region. Tectonophysics 403, 95–115.
Kontoes, C.C., Elias, P., Sykioti, O., Briole, P., Remy, D., Sachpazi, M., Veis, G., Kotsis, I., 2000. Displacement field mapping and fault modeling of the September 7th, 1999 Athens earthquake based on ERS-2 satellite radar interferometry. Geophys. Res. Lett. 27, 3989–3992.
Koukouvelas, I.K., Kokkalas, S., Xypolias, P., 2009. Surface deformation during the M_w 6.4 (8 June 2008) Movri Mountain earthquake in the Peloponnese, and its implications for the seismotectonics of western Greece. Int. Geol. Rev. 1–20. doi:10.1080/00206810802674329 iFirst Article.
Latoussakis, J., Stavrakakis, G.N., 1992. Times of increased probability of earthquakes of $M_L \geq 5.5$ in Greece diagnosed by algorithm M8. Tectonophysics 210, 315–326.
Lekkas, E., Fountoulis, I., Danamos, G., Skourtsos, E., Gouliotis, I., Mavroulis, S., Kostaki, I., 2008. Seismic fractures related to the NW Peloponnesus (SW Greece) earthquake (ML = 6,5R, 8-6-2008). 31st General Assembly, European Seismological Commission, Hersonissos, Crete, Greece, 7–12 September 2008, Programme and Abstracts, p. 320 (abstr.).
Louvari, E., Kiratzi, A.A., Papazachos, B.C., 1999. The Cephalonia Transform Fault and its extension to western Lefkada Island (Greece). Tectonophysics 308, 223–236.
Luis, J.F., 2007. Mirone: a multi-purpose tool for exploring grid data. Comput. Geosci. 33, 31–41.
Mallet, R., 1853. Third report on the facts of earthquake phenomena, 1. British Association for the Advancement of Science, London, pp. 1–176.
Massonet, D., Feigl, K., 1998. Radar interferometry and its appication to changes in the earth's surface. Rev. Geophys. 36, 441–500.
Mogi, K., 1962. Study of elastic shocks caused by the fracture of heterogeneous materials and its relations to earthquake phenomena. Bull. Earthquake Res. Inst. Tokyo Univ. 40, 125–173.
Okada, Y., 1985. Surface deformation due to shear and tensile faults in a half-space. Bull. Seismol. Soc. Am. 75, 1135–1154.
Papadopoulos, G.A., 1985. Stress-field and shallow seismic activity in the Aegean region: their tectonic implications. Quatern. Geod. 6, 65–74.
Papadopoulos, G.A., Lefkopoulos, G., 1993. Magnitude–distance relations for liquefaction in soil from earthquakes. Bull. Seismol. Soc. Am. 83, 925–938.
Papadopoulos, G.A., Plessa, A., 2000. Magnitude–distance relations for earthquake-induced landslides in Greece. Eng. Geol. 58, 377–386.
Papadopoulos, G.A., Skafida, H.G., Vassiliou, I.T., 1993. Non-linearity of the magnitude–frequency relation in the Hellenic arc–trench system and the characteristic earthquake model. J. Geophys. Res. 98, 17737–17744.
Papadopoulos, G.A., Sachpazi, M., Panopoulou, G., Stavrakakis, G., 1998. The volcanoseismic crisis of 1996–97 in Nisyros, SE Aegean Sea, Greece. Terra Nova 10, 151–154.
Papadopoulos, G.A., Vassilopoulou, A., Plessa, A., 2000. A new catalogue of historical earthquakes in the Corinth Rift, Central Greece: 480 B.C.–A.D. 1910. In:

Papadopoulos, G.A. (Ed.), Historical Earthquakes and Tsunamis in the Corinth Rift, Central Greece, pp. 9–119.
Papadopoulos, G.A., Ganas, A., Plessa, A., 2001. The Skyros Earthquake (Mw6.5) of 26 July 2001 and Precursory Seismicity Patterns in the North Aegean Sea. Bull. Seismol. Soc. Am. 92, 1141–1145, 2002.
Papadopoulos, G.A., Karastathis, V., Ganas, A., Pavlides, S., Fokaefs, A., Orfanogiannaki, K., 2003. The Lefkada, Ionian Sea (Greece), shock (M_w 6.2) of 14 August 2003: evidence for the characteristic earthquake from seismicity and ground failures. Earth Planet. Space 55, 713–718.
Papadopoulos, G.A., Matsumoto, H., Ganas, A., Karastathis, V., Pavlides, S., 2004. Deformation patterns associated with the M5.9 Athens (Greece) earthquake of 7 Sept. 1999. J. Seismol. 8, 381–394.
Papadopoulos, G.A., Karastathis, V., Kontoes, C., Papoutsis, I., Daskalaki, E., Diakogianni, G., Fokaefs, A., 2008. The earthquake of 8 June 2008 (Mw = 6.3) in NW Peloponnese, Greece: first results. 31st General Assembly, European Seismological Commission, Hersonissos, Crete, Greece, 7–12 September 2008, Programme and Abstracts, pp. 323–324 (abstr.).
Papadopoulos, G.A., Karastathis, V., Ganas, A., Charalambakis, M., Fokaefs, A., 2009. A storm of strong earthquakes in Greece during 2008. EOS Trans. Am. Geophys. Union 90 (46), 425–426 17 Nov. 2009.
Papathanassiou, G., Valkaniotis, S., Chatzipetros, A., Neofotistos, P., Sboras, S., Pavlides, S., 2008. Liquefaction-induced ground disruption triggered by the earthquake of June 8, 2008 in NW Peloponnesus, Greece. 31st General Assembly, European Seismological Commission, Hersonissos, Crete, Greece, 7–12 September 2008, Programme and Abstracts, p. 330 (abstr.).
Papazachos, B.C., 1971. Aftershock activity and aftershock risk in the area of Greece. Ann. Geofis. 24, 439–456.
Papazachos, B.C., Papazachou, C.B., 1997. The Earthquakes of Greece. Ziti Publ., Thessaloniki. 304 pp.
Papazachos, B.C., Kiratzi, A.A., Voidomatis, Ph., Papaioannou, Ch., 1984. A study on the December 1981–January 1982 seismic activity in Northen Aegean Sea. Boll. Geofis. Teor. Appl. XXVI, 101–102.
Papoutsis, I., Kontoes, C., Papadopoulos, G.A., 2008. DInSAR study of the 8 June 2008 earthquake in NW Peloponnese. 31st General Assembly, European Seismological Commission, Hersonissos, Crete, Greece, 7–12 September 2008, Programme and Abstracts, p. 323 (abstr.).
Pavlides, S.B., Tranos, M.D., 1991. Structural characteristics of two strong earthquakes in the North Aegean: Ierissos (1932) and Agios Efstratios (1968). J. Struct. Geol. 13, 205–214.
Reilinger, R.E., Ergintav, S., Bürgmann, R., McClusky, S., Lenk, O., Barka, A., Gurkan, O., Hearn, L., Feigl, K.L., Cakmak, R., Aktug, B., Ozener, H., Töksoz, M.N., 2000. Coseismic and postseismic fault slip for the 17 August 1999, M = 7.5, Izmit, Turkey earthquake. Science 289, 1519–1524.
Richardson, R.M., Solomon, S.C., 1977. Apparent stress and stress drop for intraplate earthquakes and tectonic stress in the plates. PAGEOPH 115, 317–331.
ROI_PAC, 2008. Jet Propulsion Laboratory (JPL) and the California Institute of Technology (Caltech). http://www.roipac.org/.
Romanowicz, B., Ruff, L.J., 2002. On moment-length scaling of large strike slip earthquakes and the strength of faults. Geophys. Res. Lett. 29. doi:10.1029/2001GL014479.
Roumelioti, Z., Benetatos, Ch., Kiratzi, A., Stavrakakis, G., Melis, N., 2004. A study of the 2 December 2002 (M5.5) Vartholomio (western Peloponnese, Greece) earthquake and of its largest aftershocks. Tectonophysics 387, 65–79.
Sathas, K.N., 1867. Messeonikon Seismologion tis Ellados kai idios tis Kefallinias kai Lefkados. Aion, Athens.
Scholz, C.H., 1968. Microfractures, aftershocks, and seismicity. Bull. Seismol. Soc. Am. 58, 1117–1130.
Shi, B., Brune, J.N., Zeng, Y., Anooshehpoor, A., 2003. Dynamics of earthquake normal faulting: two-dimensional lattice particle model. Bull. Seismol. Soc. Am. 93, 1179–1197.
Shieh, C.-F., Sheu, S.-Y., Shih, R.-C., 2001. Correlation between surface damage and the coseismic displacement and stress relaxation of the 1999 Chi-Chi, Taiwan earthquake. Geophys. Res. Lett. 28, 3381–3384.
Spyropoulos, P.J., 1997. Chronicle of the Earthquakes in Greece from the Ancient Time till Now. 453 pp. (In Greek).
Talebian, M., Fielding, E.J., Funning, G.J., Ghorashi, M., Jackson, J., Nazari, H., Parsons, B., Priestley, K., Rosen, P.A., Walker, R., Wright, T.J., 2004. The 2003 Bam (Iran) earthquake: rupture of a blind strike–slip fault. Geophys. Res. Lett. 31. doi:10.1029/2004GL020058.s.
Taymaz, T., Jackson, J., McKenzie, D., 1991. Active tectonics of the north and central Aegean Sea. Geophys. J. Int. 106, 433–490.
Urbancic, T.I., Trifu, C.I., Long, J.M., Young, R.P., 1992. Space–time correlations of b-values with stress release. Pure Appl. Geophys. 139, 449–462.
Utsu, T., 1965. A method for determining the value of b in a formula log $N = a - bM$ showing the magnitude–frequency relation for earthquakes. Geophys. Bull. Hokkaido Univ. 13, 99–103 (in Japanese with Engl. abstr.).
Wyss, M., 1973. Towards a physical understanding of the earthquake frequency distribution. Geophys. J. R. Astron. Soc. 31, 341–359.
Wyss, M., 2001. Locked and creeping patches along the Hayward fault, California. Geophys. Res. Lett. 28, 3537–3540.
Wyss, M., Schorlemmer, D., Wiemer, S., 2000. Mapping asperities by minima of local recurrence time: the San Jacinto–Elsinore fault zones. J. Geophys. Res. 105, 7829–7844.
Wyss, M., Sammis, C.G., Nadeau, R.M., Wiemer, S., 2004. Fractal dimension and b-value on creeping and locked patches of the San Andreas Fault near Parkfield, California. Bull. Seismol. Soc. Am. 94, 410–421.
Zhao, Y.Z., Wu, Z.L., 2008. Mapping the b-values along the Longmenshan fault zone before and after the 12 May 2008, Wenchuan, China, Ms 8.0 earthquake. Nat. Haz. Earth Syst. Sci. 8, 1375–1386.
Zygouri, V., Kokkalas, S., Xypolias, P., Koukouvelas, I.K., Papadopoulos, G.A., submitted for publication. Paleoseismological evidence from an emerging structure above a blind fault: the Nisi fault (NW–Peloponnese, Greece) as a case example.